Applied Geomatics (2023) 15:407–420
https://doi.org/10.1007/s12518-023-00501-2

ORIGINAL PAPER

# Use of time series Sentinel-1 and Sentinel-2 image for rice crop inventory in parts of Bangladesh

**Md. Abdullah Aziz**[1] · **Dipanwita Haldar**[2] · **Abhishek Danodia**[2] · **Prakash Chauhan**[3]

Received: 22 October 2022 / Accepted: 20 February 2023 / Published online: 30 March 2023


**Abstract**

Synergistic use of satellite data has an advantage over single-source data as optical, thermal, and microwave datasets. Previous studies have demonstrated the efficacy and focused mainly on the edge of the multisensory data over the stand-alone system due to primarily multi-dimension input. Crop classification and crop type mapping is the first step in the natural resource management theme, especially in agriculture. During the rainy season, accurate crop classification with crop-cultivar type mapping is the most challenging target to achieve using optical datasets. Therefore, the study's prime focus was to extract the temporal signature of rice crop types from multi-temporal SAR datasets and classify various rice crop types based on sowing timing in the dominant production zone of rice, the Jashore district of Bangladesh. Sentinel-1 datasets were used primarily for the rainy season from July to September 2018; in addition, Sentinel-2 data of October was used to understand the relationships among these datasets. The temporal signature of various types of rice and others features was interpreted. Besides, the correlation between Sentinel-1 backscatter with Sentinel-2 derived indices has been exercised to find out a comprehensive framework for selection of optical vegetation indices which may be used as a proxy of SAR or vice-versa. The classified image from Sentinel-2 has around 80% overall accuracy, and 0.71 value of kappa coefficient for rice crop type mapping was comparable to SAR (about 80% for late sown crop and slightly less for the other 2 classes); class accuracy of the rice crop is 88–90% using three-date dual-polarized data. The latter's advantage is early estimate availability during the initial crop phase when optical data is not available. Three types of rice were observed to be cultivated; these are early transplanted rice, late transplanted rice, and very late transplanted rice; among them, late transplanted rice covered a large area, and early transplanted rice covered lesser areas during the session. Sentinel-2 derived spectral indices have a higher correlation with very late rice crop type for VV backscatter than early (where the response in VH was significant probably after saturation in VV response due to matured crop) and late rice crop types. Understanding the micro and macro-scale crop structure from a multisource- remote-sensing perspective builds novelty in this research.

**Keywords** Classification · Sentinel-1 · Sentinel-2 · Rice crop type · Temporal Signature · Backscatter value

✉ Md. Abdullah Aziz
abdullahaziz.stat@brri.gov.bd

Dipanwita Haldar
dipanwita@iirs.gov.in

Abhishek Danodia
abhidanodia@iirs.gov.in

Prakash Chauhan
cssteap@iirs.gov.in

[1] Bangladesh Rice Research Institute, Gazipur 1701, Bangladesh

[2] Indian Institute of Remote Sensing, Dehradun, Uttarakhand, India

[3] The Centre for Space Science and Technology Education in Asia and the Pacific, Dehradun, India

## Introduction

Microwave remote sensing has a number of advantages over optical remote sensing, the most obvious of which is its ability to penetrate through clouds and, to some extent, rain. Second, because the microwave system is not dependent on the sun for illumination, it can operate 24 h a day. Third, microwaves can penetrate deeper into plants than EM radiation with an optical spectrum. As a result, when it is used to monitor vegetation, it can obtain surface information from the vegetation and get some signal back from the deep interaction. It can gather leaf, branch, stem, and other structural/geometric information under the surface of plants in the depths of the vegetation (Macelloni et al. 2001;

Fontanelli et al. 2013; Haldar et al. 2014a, b). Fourth, the structural qualities and dielectric properties of surface features influence the signal by the microwave sensor; therefore, this information can reflect surface attributes of objects that appear similar in optical terms but differ from a SAR perspective (Shewalkar et al. 2014). Furthermore, due to the unique specular features of rice fields under flooded surface conditions, the SAR delineation of rice fields is relatively strong (Choudhury et al. 2012). Based on temporal fluctuations in the SAR backscatter ([dB]) signal, multi-temporal SAR data may be used to retrieve the rice-growing cycle. The most popular data analysis approach for paddy rice identification is the time series analysis of SAR backscatter.

Bangladesh can be defined as a rice-growing and rice-eating country. Food security and rice security are synonymous in Bangladesh (Kabir et al. 2020). Rice is Bangladesh's primary food. In Bangladesh, rice is cultivated 78% of total net crop area (Mamun et al. 2021; Rahman et al. 2022). Bangladesh produced approximately 33.8 million tons of rice, where area coverage was about 27 million acres in 2016–2017 (BBS 2017). Rice accounts for more than 80% of the entire food supply. Rice is consumed by higher than 95% of the population, and it alone provides 76% of daily calorie and 66% of absolute protein requirements (Awal and Siddique 2011; Rahman et al. 2020).

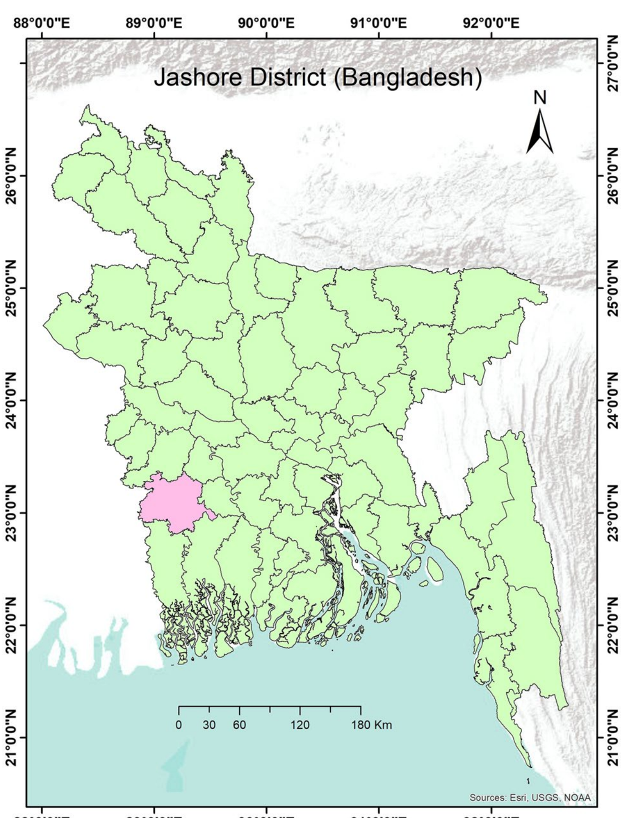


**Fig. 1** Location of Jashore district (Bangladesh)

Agricultural statistics have become increasingly important in shaping and disseminating scientific data that is relevant to practically every element of human life and beyond (Faisal et al. 2019). Due to lower economic efficiency and other characteristics of agricultural output, such as broad coverage, severe seasonality, and spatial variability, standard ground survey methods make obtaining yearly crop information difficult. Furthermore, the obtained data may become available too late for decision-makers or planners in the country to take necessary action. The application of remote sensing technology can be a practical and effective method of resolving this issue. Since remote sensing has been used to identify and extract areas, the results have been astounding. In India, technology and theory have been continuously improved and have progressed to an operational level (Chakraborty et al. 1997; Haldar et al. 2014a, b). Remote sensing technology enables scalable and unbiased estimates of rice area to support, enhance, and complement the existing system based on survey and statistical approaches (Gumma et al. 2014). Crop mapping, area estimation, monitoring system, and crop yield forecasts begin with the identification of crop types (Shewalkar et al. 2014).

Bangladesh has three rice seasons: Aus, Aman, and Boro (BRRI 2018). In 2016–2017, total Aman rice production was 13.6 million tons, about 40% of the total rice production. Aman is cultivated from June to November, but typically produced from July to October when puddling/transplanted in mid-July, peak vegetative stage (booting/flowering stage) at early to mid-September and harvested at the end of October or early November. Thus, Aman rice is a Kharif season crop during the monsoon season of south-east Asia, and most of the time, the sky remains covered by clouds.

Due to frequent cloud cover, most optical remote sensing technologies fail to detect rice during the monsoon (Nuevo et al. 2017).

Rice crop growth stages were tracked and variation was measured using single-polarization and multi-polarization SAR datasets. C-band SAR sensors have been the most appealing data source for rice mapping at a regional or continental scale in this technique since data from other SAR

**Table 1** Image date and rice cultivation condition

| Date | Expected rice growing stage |
|---|---|
| 17/07/2018 | Puddling |
| 29/07/2018 | Transplanting |
| 10/08/2018 | Tillering |
| 22/08/2018 | Panicle initiation |
| 03/09/2018 | Booting |
| 15/09/2018 | Flowering (peak vegetative stage) |

sensors is restricted by low spatial coverage or longer revisit durations (Nguyen and Wagner 2017).

The SAR-based vegetation indices were built from full polarization radar pictures to measure the rice crop growth characteristics, which was an important aspect of this work. Recent research has also focused on creating vegetation indices using dual-polarization SAR data in order to estimate biophysical parameters including soil moisture content, crop water content, and agricultural yield. However, only a small amount of effort has gone into creating hybrid indices that combine optical and SAR indices (Alebele et al. 2020).

Sentinel-1 data, which has a spatial resolution of 10 m × 10 m and a temporal resolution of every 6 days, offers a wide range of applications, even at the farm level. The European Space Agency (ESA) has recently launched two important remote sensing satellites, Sentinel-1A, and Sentinel-1B (collectively called Sentinel-1). It is equipped with a C band SAR with a central frequency of 5.405 GHz (ESA, 2013). Because of its sensitivity to background water and crop geometry, this radar frequency is essential for monitoring the lowland rice environment (Choudhury et al. 2012). Sentinel-1 can now perform all-weather, day and night global surveillance every 6 days because the two spacecraft are now 180° apart in orbit (ESA, 2013). Furthermore, Sentinel-1A has a dual-polarization imaging mode that allows it to receive both H and V backscattered polarization while transmitting one of them. When compared to the full-polarimetric mode, Sentinel-1A helps achieve superior range resolution, a larger swath, and lower data processing needs (Haldar et al. 2014a, b).

Although Sentinel-1 and Sentinel-2 have two separate wavelength-based data acquisition and the manifestation with the plant former at a macro level and later at a micro level, the later aggregate is the cause for the former SAR-based system. Both the datasets can make various applications, i.e., crop inventory, crop mapping, soil moisture, and crop yield. Also, the synergistic and conjunctive has proven to yield a more robust understanding than the sole usage in both area estimates and understanding the crop health and yield potential (McNairn et al. 2001a, b; Haldar and Patnaik 2010, 2012a, b, 2020).

Traditional ground survey methods are still being conducted in Bangladesh for area estimation, monitoring systems, and crop yield forecasting. According to a survey of the literature, there are research on rice growth monitoring and modeling using optical data, most of which are based on MODIS data; no studies were found on crop type identification, monitoring, and modeling its growth by SAR data. Thus, this study aims to extract the temporal signatures of rice types using the Sentinel-1 satellite and classify them based on unique temporal signatures to determine their transplanting sequence. Also, evaluate the

**Table 2** Spectral indices used in the study and their formula

| Sl No | Indices | Index full name | Formula | Citations |
|---|---|---|---|---|
| 1 | NDVI | Normalized difference vegetation index | NDVI = (NIR-Red)/ ( NIR + Red) | (Zuzulova and Vido 2018) |
| 2 | SAVI | Soil-adjusted vegetation index | SAVI = (1 + L) (NIR-Red)/(NIR + Red + L) where L is soil condition index | Xue and Su 2017 |
| 3 | EVI | Enhanced vegetation index | $EVI = (TM_4 - TM_3)(1 + L)/( TM_4 - C_1 TM_3 + C_2 TM + L)$ | Xue and Su 2017 |
| 4 | SLAVI | Specific leaf area vegetation index | SLAVI = NIR/(RED + SWIR) | IDB, 2021 |
| 5 | NDRE | Normalized difference red edge (NDRE) | $NDRE = (R_{790} - R_{720})/(R_{790} + R_{720})$ | Barnes et al. 2000 |
| 6 | REIP | Red edge inflection point (REIP) | $REIP = 700 + 40[\{(p_{667+}P_{782})/2\} - p_{702}]/p_{738} - p_{702}$ | Herrmann et al. 2010 |
| 7 | RNDVI | Renormalized index of normalized difference vegetation index | RNDV = (\|NDVIt1\|–NDVIt2\|)/(\|NDVIt1\| + \|NDVIt2\|) where t1 and t2 refer to the acquisition date of each scene in which the derivative NDVI | Li et al. 2016 |
| 8 | NDII | Normalized difference infrared Index | $NDII = (\rho_{0.85} - \rho_{01.65})/ (\rho_{0.85+}\rho_{01.65})$ | Sriwongsitanon et al. 2015 |
| 9 | NDSI | Normalized difference snow index (NDSI) | $(Green_{0.53} - SWIR_{1.65)}/(Green_{0.53} + SWIR_{1.65)}$ | Sibandze et al. 2014 |
| 10 | SIWSI | Shortwave infrared water stress index | SIWSI = (ρSWIR − ρNIR)/(ρSWIR + ρNIR) | Olsen et al. 2013 |
| 11 | ARVI | Atmospherically resistant vegetation index | NIR − RED − *y*(RED − BLUE) NIR + RED − *y* (RED − BLUE y = quotient derived from the components of atmospheric reflectance in the blue and red channel | IDB, 2020a, b |
| 12 | ARVI2 | Adjusted resistant vegetation index 2 | $ARVI2 = -0.18 + 1.17 \times (R_{NIR} - R_{Red}/ R_{NIR} + R_{Red})$ | Adamu et al. 2018 |
| 13 | GARI | Green atmospherically resistant vegetation index (GARI) | GARI = (NIR-[Green-γ(Blue-Red)])/ (NIR + [Green-γ(BlueRed)]) | Susantoro et al. 2018 |

relationship between SAR-based backscatter values with different optical dataset-based indices for effective monitoring of the crop during availability of the dual-source data or anyone.

## Study area

Jashore district is a very prospective area for Aman rice production. In 2016–2017, total Aman area of Jashore was about 1200 sq. km and production of 346,090 metric tons (BBS 2017). Jashore district is located in between 22°48′ and 23°22′ north latitudes and in between 88°51' and 89°34' east longitudes (Fig. 1). It is surrounded by two districts named Jhenaidah and Magura on the north and two other districts on the south called, Satkhira and Khulna, and another two districts on the eastern side named Narail and Khulna. On the western side, it is surrounded by the West Bengal state of India. Jashore district area is about 2500 sq. km, and the total population is about 2.4 million (Banglapedia 2020). Jashore district has excellent agricultural potential under the High Ganges River Floodplain agrological zone. Major crops in Jashore are rice, wheat, jute, maize, and others (BBS, 2017).

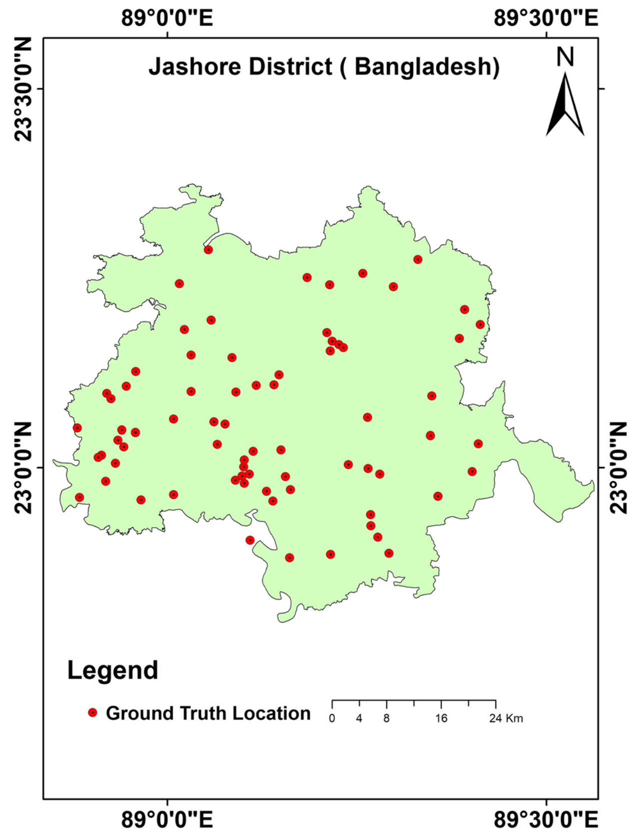


**Fig. 2** Jashore district (Bangladesh)

## Materials and methods

### Datasets

#### Sentinel-1

Sentinel-1 launch by European Space Agency (ESA) on 2014 (https://scihub.copernicus.eu/dhus/) having 10-m spatial resolution and C-band (3.75–7.5 cm) SAR data (ESA 2013).

Sentinel-1A data were downloaded from the European Space Agency (ESA) for Kharif seasons from 17 July 2018 to 15 September 2018, where polarizations were VV + VH, product type, and sensor mode were GRD and IW, respectively. Sentinel 1 data collection dates with rice-growing status are shown in Table 1.

#### Sentinel-2

Sentinel-2, is an optical sensor also launched by European Space Agency (ESA) having 10-m spatial resolution (Park et al. 2017 and ESA, 2021). In this study stating and demonstrating the conjunctive use of SAR with optical, in peak rainy season, optical data is unavailable; hence, SAR data were used, and post-rain, optical data is used; in past studies, the synergy has been established, and hence, the datasets may not be repeated and used as surrogate for others (Haldar and Patnaik 2010, 2012a, b, 2020).

Due to maximum cloud coverage during monsoon season, only one scene of Sentinel-2 was available in the late season during mid-October 2018 (17 October 2018). Nevertheless, this was found useful as this coincides with the entire growth stage of the crop and could be highly correlated with the multiple scattering mechanisms. The cloud-free single scene of Sentinel-2A, level 2 product which is corrected surface reflectance (ESA, 2022) was downloaded (https://scihub.copernicus.eu/dhus/) for preparing level 1 crop classification and various spectral vegetation indices to be studied conjunctively with the SAR data. Spectral vegetation indices depict useful information about crop growth, crop condition, crop biophysical parameters relationship, and others (Thenkabail et al. 1999). These were used to understand crop growth progress with the multi-temporal dual-polarized SAR data.

A combination of visible and short-wave infrared bands generated thirteen spectral vegetation indices. A further correlation was derived with early, late, and late rice types backscatter values in VV and VH polarization. Table 2 illustrates the list of spectral indices and their formula.

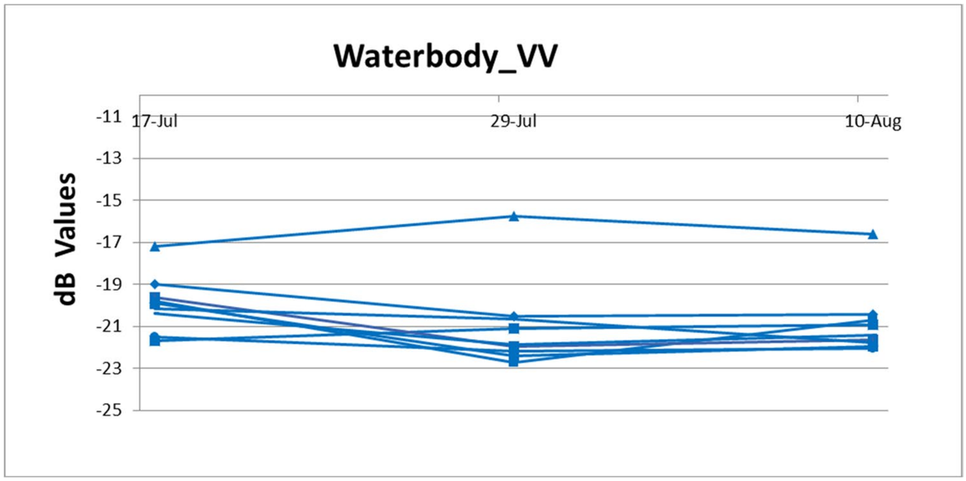


**Fig. 3** Temporal signature of water body using VV polarization by various GT points

## Ground truth data

Ground truth data is required to train the classifiers and assess the map's accuracy (McNairn et al. 2014). Ground truth (GT) data was gathered in time with satellite passes. A GPS receiver was utilized to mark the coordinates of the rice crop field. Rice crop fields that covered more than three to five hectares over a continuous length were frequently sampled for this study. From the latter week of September to the first week of October, GPS data were gathered via field survey on a total of 50 rice fields and 5 fallow fields. Date of crop planting and transplanting as well as crop stage were gathered as plant parameters. Additional features from Google Earth, including homestead, water body, orchard, big city, etc., totaled 18 points of latitude and longitude. The classification model was trained using 70% of the ground truth data, and the final map's accuracy was tested using the remaining 30%. Figure 2 shows the ground truth location.

## Pre-processing of SAR data

The pre-processing of Sentinel-1A data includes five main steps: (1) orbit file correction; (2) speckle-noise filtering using Lee sigma filter and $5 \times 5$ window; the $5 \times 5$ window has been established with a lot of past datasets, and this is optimum for many agricultural applications (Chakraborty et al. 1997, Haldar and Patnaik 2010, 2019); (3) radiometric calibration to convert digital pixel values of VH/VV amplitude into sigma naught (σ°) values; (4) terrain correction; and (5) data conversion from sigma naught (σ°) values to dB values. These scenes were then stacked into a multi-temporal composite scene to obtain the stacked data of the six dates.

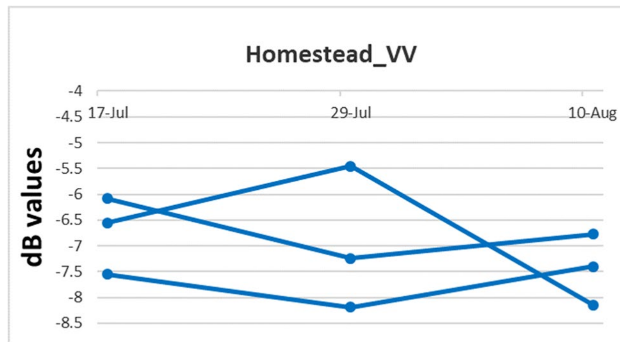


**Fig. 4** Temporal signature of homestead using VV polarization by various GT points

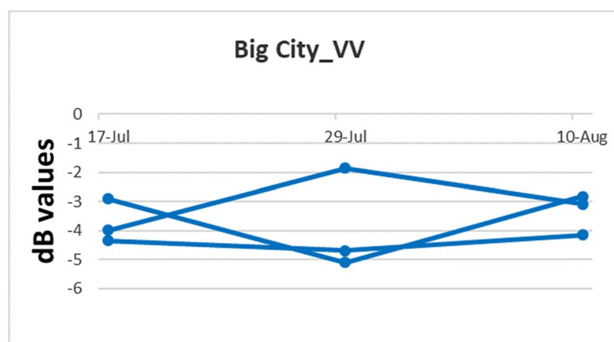


**Fig. 5** Temporal signature of big city using VV polarization by various GT points

## Generation of temporal signature and classification approach

Three days' composite of VV polarization were loaded for visualization and extraction of the signature using ENVI software, overlaying the GT points and preparing ROI

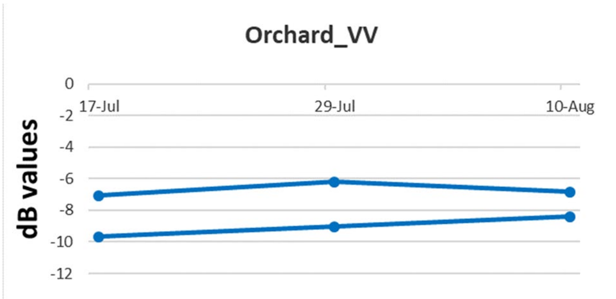


**Fig. 6** Temporal signature of orchard body using VV polarization by various GT points

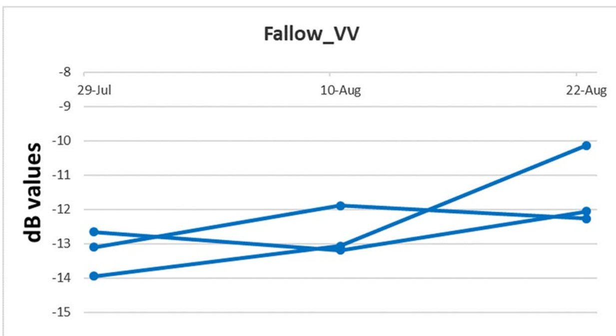


**Fig. 7** Temporal signature of fallow body using VV polarization by various GT points

(region of interest) of those locations. Statistics of those ROIs have been taken for all bands (six days) for both VV and VH polarization. Temporal signature of rice (early, late, and very late transplanted rice) and non-rice (water body, urban, homestead, fallow land, and others) have been prepared eventually by thresholding dB value of each feature, extracted for input and preparation of a decision tree.

When SAR data was employed in prior studies, decision tree (DT) classification provided superior crop discrimination and classification accuracy (Friedl and Brodley 1997). Our findings backed up previous research, and when SAR data was added, DT performed well in crop classification (Haldar et al. 2014a, b; Sahu et al. 2018; Dave et al. 2017; H. McNairn et al. 2014). The linear discriminating functions that determine the decision tree, which consists of a set of decision rules, were utilized to test each node. Sentinel-1 datasets' VV and VH polarizations were used to construct decision algorithms based on temporal backscattering responses of different crops (Shanmugapriya et al. 2020). The decision tree was used to obtain the output at each level, and the classed image was obtained as a result. For accuracy assessment, the remaining GT points were taken to prepare ROI (region of interest) and merged. A confusion matrix was produced, and an accuracy assessment table was found.

## Preparation of crop classification map by optical image

Red, green, and NIR bands created the false color composite (FCC). Crop classification maps of the study area were prepared by supervised classification using a maximum likelihood classifier (MLC) (Singh et al. 2020).

## Evaluate the response between backscatter values with various optical-based indices

A correlation analysis was performed between SAR-derived backscatter value and optical dataset-derived vegetation indices to know the relationship between the datasets and find the possible way to use one data as a proxy for other data. In this context, thirteen spectral indices were generated using Sentinel-2, and linear regression equations have been developed using backscatter values. This relationship was performed for rice crop types as early, late, and very late-type to illustrate the perspective of SAR and optical data as a proxy.

Whenever one data is missing, we can use the surrogate by another, and this relationship has been established in the past (Ghaffarian et al. 2018). To

**Fig. 8** Temporal signature of early transplanted rice using VH polarization by various GT points

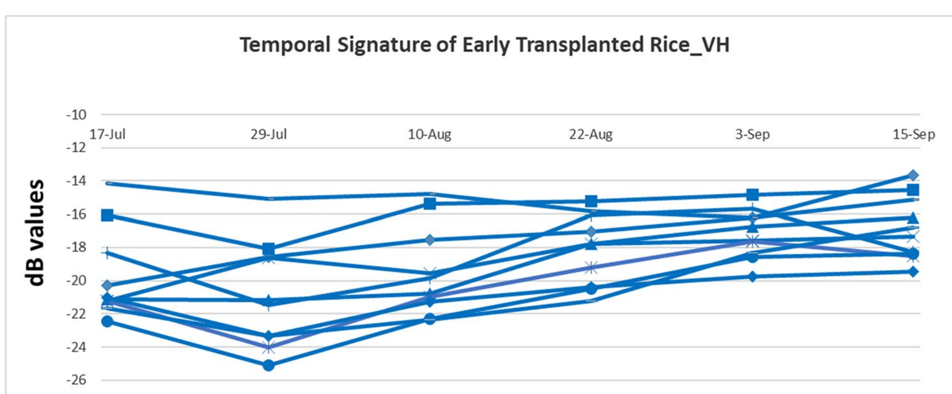

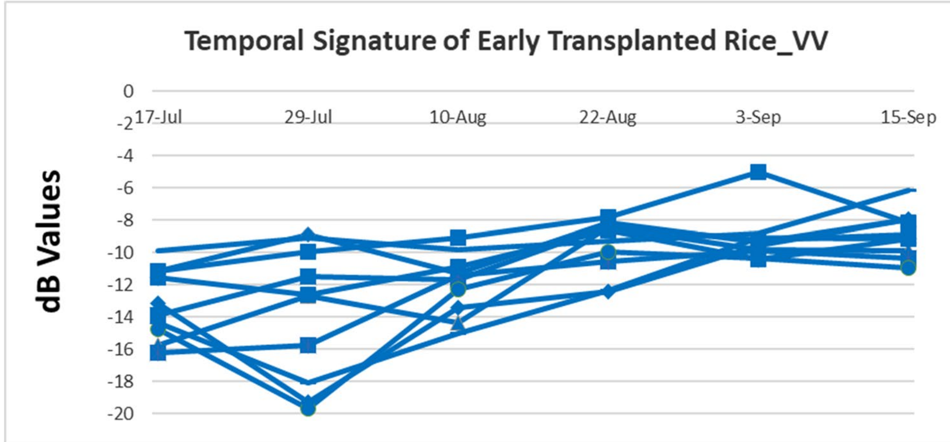


**Fig. 9** Temporal signature of early transplanted rice using VV polarization by various GT points

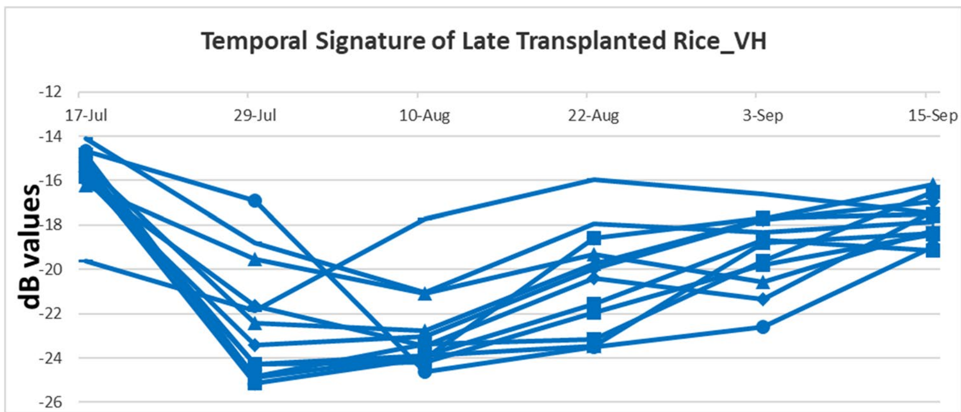


**Fig. 10** Temporal signature of late transplanted rice using VH polarization by various GT points

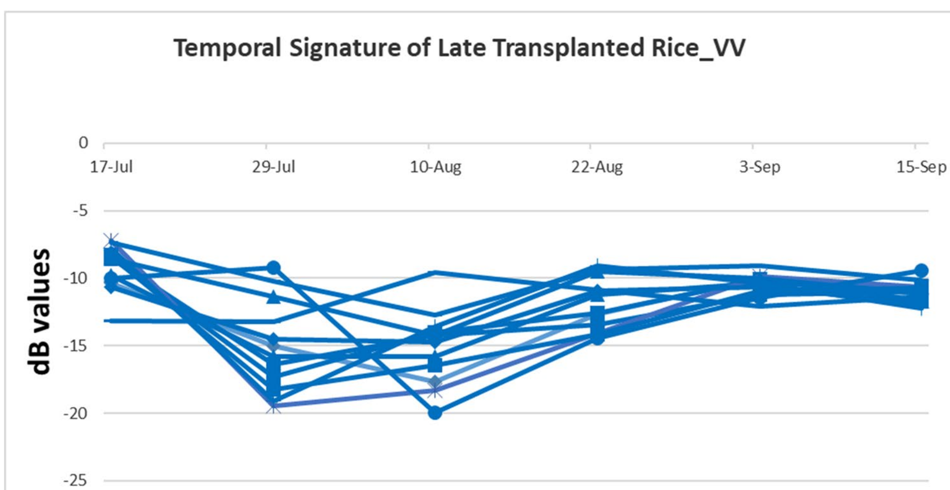


**Fig. 11** Temporal signature of late transplanted rice using VV polarization by various GT points

evaluate the relationship between SAR-based backscatter values and various optical-based indices were extracted from the Sentinel-2 data. A total of thirteen indices, i.e., NDVI, SAVI, EVI, SLAVI, NDRE, REIP, RNDVI, NDII, NDSI, SIWSI, ARVI, ARVI2, and GARI, were derived from the Sentinel-2 data. Then all GT points based value extraction of all indices was made.

To find out the relationship between SAR-based backscatter and various optical-based indices values, one simple

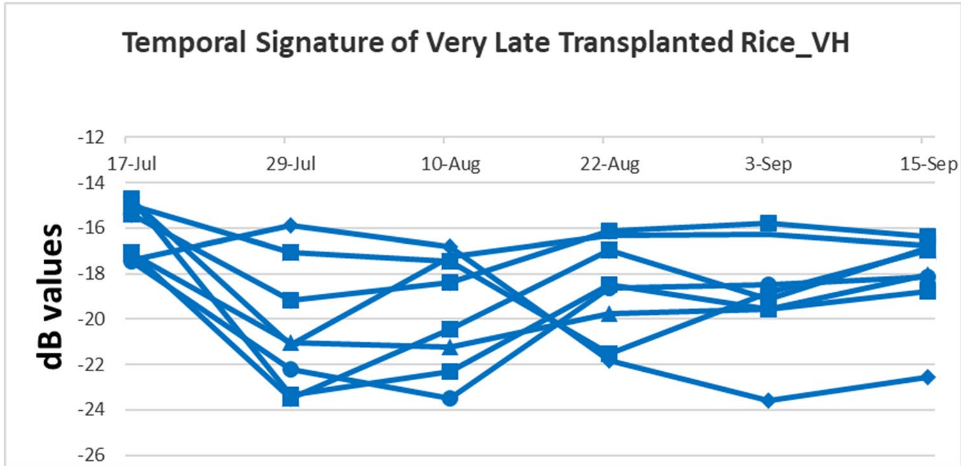


**Fig. 12** Temporal signature of very late transplanted rice using VH polarization by various GT points

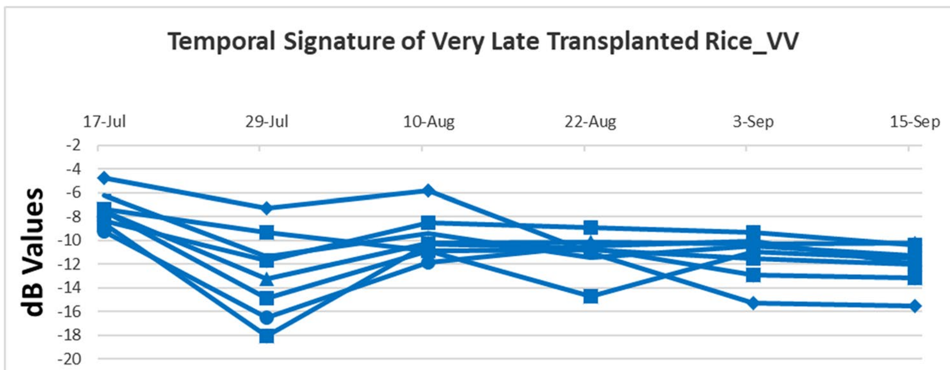


**Fig. 13** Temporal signature of very late transplanted rice using VV polarization by various GT points

linear model was used to evaluate the relationship between VV and VH with each of the 13 indexes, for each of the 3 dates and each of the three rice types, resulting in 234 different models.

The formula of the linear regression model is.

$Y = a + bx + \epsilon$.

Where $Y$ is dependent variable, $a$ is intercept, $b$ is slope, $x$ is independent variable, and $\epsilon$ is residual.

Here, the SAR-based backscatter value is considered as a dependent variable evaluating the backscatter arising due to the scattering attributed to the above-ground biomass (scattering elements—tillers and leaves standing above the ponded water surface). However, optical indices as an independent variable are the basis for considering; this is a more fundamental attribute to the rice crop health at the micro-scale level. The chlorophyll-based indices; leaf water status; red edge, which results in the macrostructures sensed by SAR and others; and also the best-fitted model were selected. Observations of early, late and very late transplanted rice are respectively area 10, 12 and 08.

## Results and discussion

### Temporal signature

Temporal signatures were derived from time sequences of observations of the Sentinel-1 data. They are particularly significant for monitoring the earth's environmental changes (Liang et al. 2008). The backscatter values of non-rice features of the study area (water body, big city, fallow land) remain more or less same over time (a little bit changes due to some minor factors). Their backscatter values are depicted in Figs. 3, 4, 5, 6, and 7 for various GT points.

Paddy has a distinct temporal profile that makes it easier to distinguish from other crops due to the presence of standing background water for a major portion of the paddy lifecycle. The only difference between VV and VH is the intensity (Chakraborty et al. 1997); the cross-polarized (VH) response starts at a significantly lower value and has a much larger range than the co-pol (VV) response.

Rice crop is cultivated/transplanted, understanding water condition for most of its growth. Due to surface scattering predominantly from standing water, too short and very low

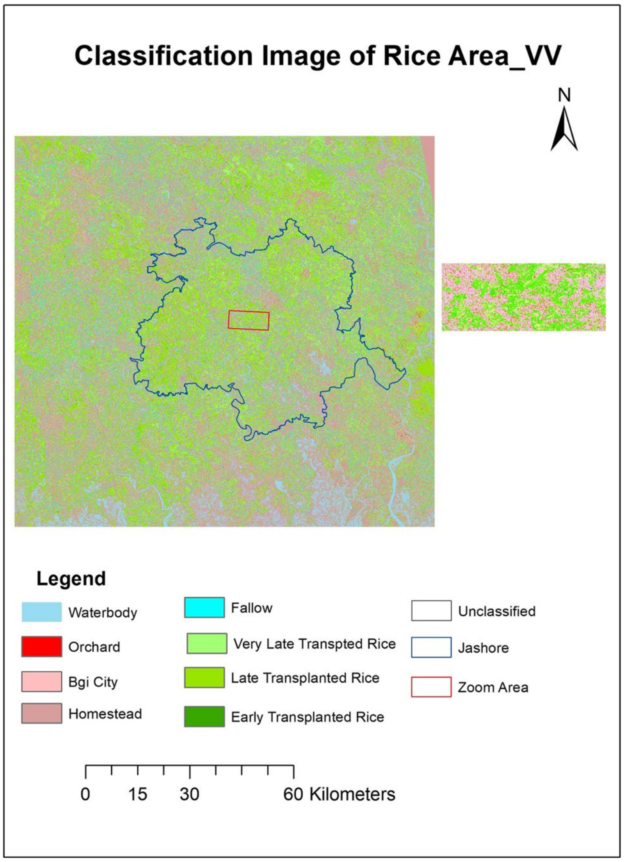


**Fig. 14** Classification output of rice area using VV polarization by various GT points

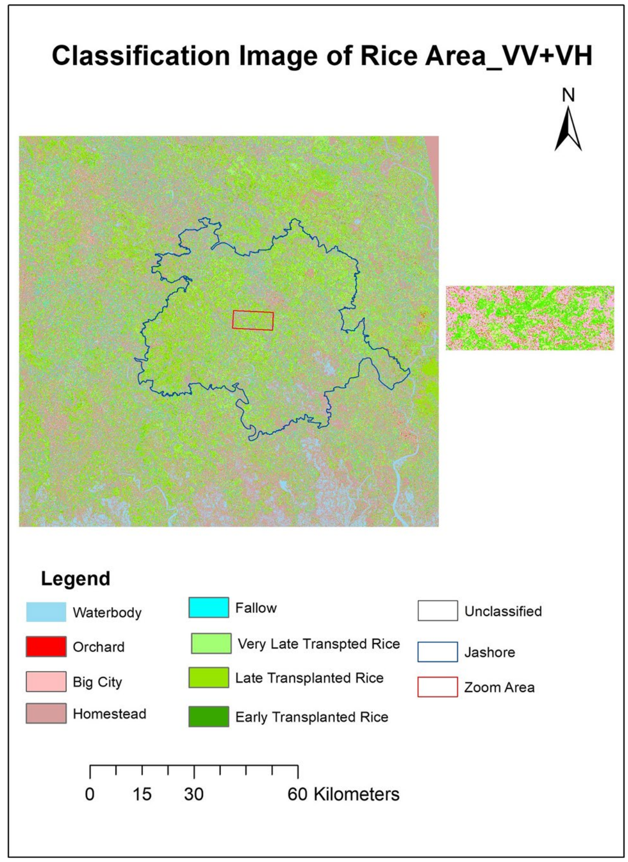


**Fig. 15** Classification output of rice area using VV and VH polarization by various GT points

backscatter value (dB) of plant height was found during rice transplanting. However, plants' height increases with time to the peak vegetative stage (booting/flowering stage). Also, backscatter increases due to double bounce scattering up to the peak vegetative stage; after that, it remains constant.

In early transplanted rice, the backscatter of the paddy for VH polarization from − 25 to − 13 dB and for VV polarization ranged from − 19 to − 5 dB, temporal signatures (Figs. 8 and 9) followed an increasing trend of dB values, and this class rice was probably transplanted from early to mid-July. In late transplanted rice, for VH polarization, the backscatter of the paddy ranged from − 25 to − 14 dB, and for VV polarization, the backscatter of the paddy ranged from − 19 to − 7 dB; temporal signatures first decreased after that increased, which are illustrated in Figs. 10 and 11, and rice probably transplanted during late July to early August.

In very late transplanted rice, the backscatter of the paddy for VH polarization was from − 24 to − 14 dB and for VV polarization ranged from − 18 to − 4 dB. The temporal trends first decreased, then a very slowly increasing trend was observed (Figs. 12 and 13), and this rice class was probably transplanted from late August to early September.

## Rice classification approach by SAR data

Two classified outputs were prepared, and one decision tree was prepared using multidate only VV-polarization (Fig. 14). Another classified output (Fig. 15) decision tree

**Table 3** Accuracy table for rice classified image

| | | | | |
|---|---|---|---|---|
| Overall Accuracy | | 79.86% | | |
| Kappa Coefficient | | 0.71 | | |
| Class | Prod. Accuracy (%) | User. Accuracy (% ) | Prod. Accuracy (Pixels) | User Accuracy (Pixels) |
| Waterbody | 100 | 100 | 13/13 | 13/13 |
| Homestead | 78.57 | 100 | 11/14 | 11/11 |
| Big city | 100 | 75 | 9/9 | 9/12 |
| Orchard | 100 | 50 | 7/7 | 7/14 |
| Fallow | 100 | 75 | 9/9 | 9/12 |
| Early trans. rice | 81.63 | 82.76 | 120/147 | 120/145 |
| Late trans. rice | 70.76 | 69.74 | 53/75 | 53/76 |
| Very late trans. rice | 68.97 | 100 | 20/29 | 20/20 |

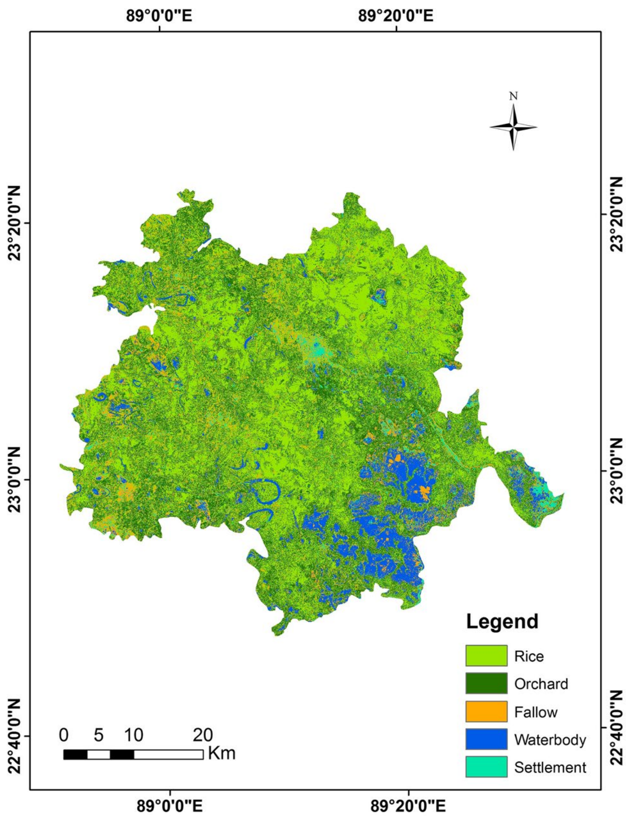


**Fig. 16** Land use land cover map of the study area

for rice was prepared using VV and VH polarizations. It was found that the classified output by using only the VV polarization had many regions unclassified. Still, the classified result using both VV and VH polarization could cover more rice areas. There is a distinct difference in accuracy when using only VV polarization (overall accuracy of 70.24%). The classified output using both VV and VH polarization resulted in an overall accuracy of 79.86% (Table 3). Thus, we can consider VV + VH classified output for analysis and illustration.

Image showing three types of rice (based on sowing date) are found, these are (i) early transplanted, (ii) late transplanted, and (iii) very late transplanted rice.

Early transplanted rice probably gets transplanted from mid to late July with the onset of the southwest monsoon, late transplanted rice from late July to early August, and very late transplanted rice from late August to early September. Late transplanted rice covers a large area, and early transplanted rice covers very few locations. Thus, most farmers transplant rice between late July and early August.

**Table 4** The results of the linear regression table for early transplanted rice backscatter value with various optical indices

| Indicies | VH ploarization | | | | | | | | | | | | | | | VV ploarization | | | | | | | | | | | | | | |
|---|---|---|---|---|---|---|---|---|---|---|---|---|---|---|---|---|---|---|---|---|---|---|---|---|---|---|---|---|---|---|
| | 17-Jul | | | | | 10-Aug | | | | | 15-Sep | | | | | 17-Jul | | | | | 10-Aug | | | | | 15-Sep | | | | |
| | Slope | SE | Inter-cept | SE | R square | Slope | SE | Inter-cept | SE | R square | Slope | SE | Inter-cept | SE | R square | Slope | SE | Inter-cept | SE | R square | Slope | SE | Inter-cept | SE | R square | Slope | SE | Inter-cept | SE | R square |
| NDVI | 2.97 | 6.36 | −21.18 | 3.49 | 0.03 | −2.82 | 6.27 | −17.79 | 3.44 | 0.03 | −6.85 | 3.15 | −12.94 | 1.73 | 0.40 | −3.63 | 5.04 | −11.29 | 2.77 | 0.07 | 1.04 | 4.39 | −12.31 | 2.41 | 0.01 | −2.52 | 3.12 | −7.64 | 1.71 | 0.01 |
| SAVI | 1.98 | 4.24 | −21.18 | 3.49 | 0.03 | −1.88 | 4.18 | −17.79 | 3.44 | 0.03 | −4.57 | 2.10 | −12.94 | 1.73 | 0.40 | −2.42 | 3.36 | −11.29 | 2.77 | 0.07 | 0.69 | 2.93 | −12.31 | 2.41 | 0.01 | −1.68 | 2.08 | −7.64 | 1.71 | 0.09 |
| EVI | −0.45 | 0.90 | −20.72 | 2.42 | 0.03 | 0.11 | 0.90 | −18.99 | 2.43 | 0.00 | 0.77 | 0.50 | −14.66 | 1.35 | 0.25 | 0.28 | 0.74 | −12.51 | 1.98 | 0.02 | −0.48 | 0.60 | −12.95 | 1.61 | 0.08 | 0.35 | 0.44 | −8.11 | 1.19 | 0.08 |
| SLAVI | 1.00 | 2.13 | −21.57 | 4.27 | 0.03 | −0.78 | 2.11 | −17.76 | 4.23 | 0.02 | −2.11 | 1.11 | −12.43 | 2.22 | 0.34 | −1.01 | 1.71 | −11.23 | 3.43 | 0.05 | 0.78 | 1.45 | −13.29 | 2.90 | 0.04 | −0.98 | 1.03 | −7.06 | 2.06 | 0.11 |
| NDRE | 3.03 | 7.12 | −20.98 | 3.36 | 0.03 | −3.49 | 6.98 | −17.70 | 3.29 | 0.03 | −7.90 | 3.43 | −12.98 | 1.62 | 0.43 | −3.93 | 5.64 | −11.42 | 2.66 | 0.06 | 1.14 | 4.90 | −12.28 | 2.31 | 0.01 | −2.88 | 3.48 | −7.67 | 1.64 | 0.09 |
| REIP | 0.05 | 0.16 | −52.32 | 118.09 | 0.01 | −0.09 | 0.16 | 45.93 | 114.35 | 0.04 | −0.18 | 0.08 | 112.42 | 56.93 | 0.42 | −0.12 | 0.12 | 71.02 | 90.66 | 0.11 | 0.01 | 0.11 | −15.42 | 80.99 | 0.00 | −0.07 | 0.08 | 40.21 | 57.05 | 0.10 |
| RNDVI | 4.24 | 9.05 | −21.09 | 3.29 | 0.03 | −4.35 | 8.91 | −17.77 | 3.24 | 0.03 | −10.13 | 4.36 | −13.03 | 1.59 | 0.44 | −4.47 | 7.25 | −11.65 | 2.64 | 0.05 | 1.70 | 6.24 | −12.36 | 2.27 | 0.01 | −3.61 | 4.44 | −7.71 | 1.62 | 0.09 |
| NDII | 13.50 | 22.28 | −24.22 | 7.66 | 0.05 | 8.15 | 22.31 | −22.05 | 7.67 | 0.02 | 1.06 | 14.42 | −16.90 | 4.96 | 0.00 | 3.85 | 18.44 | −14.51 | 6.34 | 0.01 | 16.17 | 14.35 | −17.28 | 4.93 | 0.15 | −4.68 | 11.41 | −7.37 | 3.92 | 0.02 |
| NDSI | 11.38 | 32.08 | −23.81 | 11.86 | 0.02 | −15.22 | 31.37 | −13.67 | 11.60 | 0.03 | −28.34 | 17.40 | −6.10 | 6.43 | 0.27 | −16.62 | 25.43 | −7.08 | 9.40 | 0.06 | 6.15 | 21.96 | −14.03 | 8.12 | 0.01 | −16.15 | 15.18 | −3.02 | 5.61 | 0.14 |
| SIWSI | 10.24 | 22.91 | −23.61 | 8.98 | 0.03 | −3.87 | 22.85 | −17.77 | 8.96 | 0.00 | −8.78 | 14.29 | −13.12 | 5.60 | 0.05 | −4.26 | 18.74 | −11.53 | 7.35 | 0.01 | 7.37 | 15.61 | −14.64 | 6.12 | 0.03 | −7.44 | 11.40 | −6.07 | 4.47 | 0.06 |
| ARVI | 4.42 | 8.95 | −23.15 | 7.21 | 0.03 | −4.09 | 8.84 | −16.01 | 7.12 | 0.03 | −9.58 | 4.47 | −8.90 | 3.60 | 0.40 | −4.30 | 7.19 | −9.77 | 5.79 | 0.05 | 1.88 | 6.17 | −13.26 | 4.97 | 0.01 | −3.56 | 4.40 | −6.13 | 3.55 | 0.09 |
| ARVI2 | −3.88 | 3.32 | −19.23 | 1.50 | 0.22 | −8.95 | 2.89 | −16.71 | 1.31 | 0.66 | −6.94 | 4.51 | −14.53 | 2.04 | 0.32 | −9.34 | 2.99 | −9.59 | 1.35 | 0.66 | −2.26 | 4.11 | −11.33 | 1.86 | 0.06 | −6.58 | 1.41 | −6.40 | 0.64 | 0.81 |
| GARI | 0.04 | 1.25 | −19.68 | 2.15 | 0.00 | −1.04 | 1.16 | −17.70 | 2.01 | 0.10 | −1.21 | 0.64 | −14.69 | 1.10 | 0.34 | −1.01 | 0.93 | −11.66 | 1.61 | 0.14 | −0.59 | 0.82 | −10.87 | 1.42 | 0.07 | −0.44 | 0.61 | −8.30 | 1.05 | 0.07 |

**Table 5** The results of the linear regression table for late transplanted rice backscatter value with various optical indices

| | VH ploarization | | | | | | | | | | | | | | | VV ploarization | | | | | | | | | | | | | | |
|---|---|---|---|---|---|---|---|---|---|---|---|---|---|---|---|---|---|---|---|---|---|---|---|---|---|---|---|---|---|---|
| | 17-Jul | | | | | 10-Aug | | | | | 15-Sep | | | | | 17-Jul | | | | | 10-Aug | | | | | 15-Sep | | | | |
| Indicies | Slope | SE | Inter-cept | SE | R square | Slope | SE | Inter-cept | SE | R square | Slope | SE | Inter-cept | SE | R square | Slope | SE | Inter-cept | SE | R square | Slope | SE | Inter-cept | SE | R square | Slope | SE | Inter-cept | SE | R square |
| NDVI | −8.77 | 7.39 | −10.11 | 4.73 | 0.14 | 2.05 | 10.89 | −24.21 | 6.97 | 0.00 | −1.53 | 5.30 | −16.74 | 3.39 | 0.01 | −11.29 | 9.02 | −2.06 | 5.77 | 0.15 | −8.38 | 15.80 | −9.86 | 10.10 | 0.03 | −0.85 | 4.54 | −10.50 | 2.90 | 0.00 |
| SAVI | −5.84 | 4.93 | −10.11 | 4.73 | 0.14 | 1.37 | 7.26 | −24.21 | 6.96 | 0.00 | −1.02 | 3.54 | −16.74 | 3.39 | 0.01 | −7.52 | 6.02 | −2.06 | 5.77 | 0.15 | −5.59 | 10.53 | −9.86 | 10.10 | 0.03 | −0.57 | 3.03 | −10.50 | 2.90 | 0.00 |
| EVI | 0.41 | 0.40 | −14.20 | 1.50 | 0.11 | −0.29 | 0.57 | −23.96 | 2.15 | 0.03 | −0.16 | 0.28 | −18.29 | 1.04 | 0.04 | 0.31 | 0.50 | −8.14 | 1.91 | 0.04 | 0.51 | 0.83 | −13.35 | 3.14 | 0.04 | 0.03 | 0.24 | −10.94 | 0.91 | 0.00 |
| SLAVI | −1.30 | 1.11 | −12.51 | 2.75 | 0.13 | 0.21 | 1.63 | −23.42 | 4.05 | 0.00 | −0.53 | 0.78 | −16.42 | 1.93 | 0.05 | −1.72 | 1.35 | −5.04 | 3.34 | 0.15 | −1.11 | 2.37 | −12.48 | 5.89 | 0.02 | −0.17 | 0.68 | −10.62 | 1.68 | 0.01 |
| NDRE | −8.83 | 7.01 | −10.79 | 3.91 | 0.15 | 1.98 | 10.41 | −24.01 | 5.81 | 0.00 | −2.15 | 5.04 | −16.52 | 2.82 | 0.02 | −12.77 | 8.32 | −2.17 | 4.65 | 0.21 | −5.46 | 15.23 | −12.16 | 8.50 | 0.01 | −1.69 | 4.31 | −10.11 | 2.41 | 0.02 |
| REIP | −0.22 | 0.21 | 141.80 | 154.48 | 0.10 | 0.07 | 0.31 | −77.43 | 223.24 | 0.01 | −0.11 | 0.15 | 65.99 | 105.73 | 0.07 | −0.32 | 0.25 | 221.53 | 185.30 | 0.15 | 0.04 | 0.45 | −46.70 | 329.06 | 0.00 | −0.10 | 0.12 | 59.98 | 90.30 | 0.06 |
| RNDVI | −10.47 | 8.23 | −11.16 | 3.59 | 0.15 | 2.32 | 12.25 | −23.91 | 5.34 | 0.00 | −1.65 | 5.97 | −17.00 | 2.60 | 0.01 | −15.02 | 9.79 | −2.75 | 4.27 | 0.21 | −7.14 | 17.89 | −12.11 | 7.79 | 0.02 | −1.76 | 5.08 | −10.29 | 2.21 | 0.01 |
| NDII | −8.72 | 10.51 | −12.38 | 4.02 | 0.07 | −2.56 | 14.94 | −21.94 | 5.71 | 0.00 | −11.54 | 6.44 | −13.78 | 2.46 | 0.22 | −11.32 | 12.86 | −4.95 | 4.92 | 0.08 | −8.74 | 21.80 | −11.88 | 8.33 | 0.02 | −2.51 | 6.18 | −10.09 | 2.36 | 0.02 |
| NDSI | −16.09 | 14.96 | −9.30 | 5.96 | 0.11 | −1.87 | 21.81 | −22.17 | 8.68 | 0.00 | −7.82 | 10.33 | −14.61 | 4.11 | 0.06 | −30.33 | 16.73 | 2.80 | 6.66 | 0.27 | −24.75 | 30.99 | −5.37 | 12.34 | 0.07 | 1.62 | 9.08 | −11.69 | 3.61 | 0.00 |
| SIWSI | 0.68 | 1.18 | −15.91 | 0.57 | 0.05 | 1.00 | 2.42 | −23.67 | 1.16 | 0.03 | 2.28 | 2.50 | −18.70 | 1.20 | 0.12 | 2.46 | 2.74 | −10.12 | 1.32 | 0.12 | −3.21 | 4.01 | −14.23 | 1.93 | 0.10 | 0.79 | 1.24 | −11.55 | 0.60 | 0.06 |
| ARVI | −7.95 | 6.82 | −8.59 | 6.11 | 0.13 | −0.46 | 10.05 | −22.50 | 8.99 | 0.00 | −2.64 | 4.83 | −15.36 | 4.32 | 0.03 | −11.23 | 8.19 | 0.78 | 7.32 | 0.17 | −7.36 | 14.57 | −8.62 | 13.03 | 0.03 | −1.20 | 4.17 | −9.98 | 3.73 | 0.01 |
| ARVI2 | 0.68 | 1.18 | −15.91 | 0.57 | 0.05 | 1.00 | 2.42 | −23.67 | 1.16 | 0.03 | 2.28 | 2.50 | −18.70 | 1.20 | 0.12 | 2.46 | 2.74 | −10.12 | 1.32 | 0.12 | −3.21 | 4.01 | −14.23 | 1.93 | 0.10 | 0.79 | 1.24 | −11.55 | 0.60 | 0.06 |
| GARI | 3.43 | 3.46 | −21.41 | 5.79 | 0.11 | −2.78 | 4.92 | −18.28 | 8.23 | 0.03 | 0.41 | 2.44 | −18.40 | 4.08 | 0.00 | 4.37 | 4.24 | −16.53 | 7.10 | 0.10 | 3.48 | 7.26 | −21.00 | 12.16 | 0.02 | −0.30 | 2.08 | −10.55 | 0.72 | 0.00 |

**Table 6** The results of the linear regression table for very late transplanted rice backscatter value with various optical indices

| | VH ploarization | | | | | | | | | | | | | | | VV ploarization | | | | | | | | | | | | | | |
|---|---|---|---|---|---|---|---|---|---|---|---|---|---|---|---|---|---|---|---|---|---|---|---|---|---|---|---|---|---|---|
| | 17-Jul | | | | | 10-Aug | | | | | 15-Sep | | | | | 17-Jul | | | | | 10-Aug | | | | | 15-Sep | | | | |
| Indicies | Slope | SE | Inter-cept | SE | R square | Slope | SE | Inter-cept | SE | R square | Slope | SE | Inter-cept | SE | R square | Slope | SE | Inter-cept | SE | R square | Slope | SE | Inter-cept | SE | R square | Slope | SE | Inter-cept | SE | R square |
| NDVI | −1.29 | 11.59 | −15.52 | 7.11 | 0.03 | −9.14 | 23.77 | −14.43 | 14.58 | 0.03 | −13.19 | 18.97 | −10.18 | 11.64 | 0.09 | 8.22 | 13.22 | −12.66 | 8.11 | 0.04 | −9.02 | 18.81 | −4.26 | 11.54 | 0.04 | −16.34 | 15.62 | −2.12 | 9.58 | 0.18 |
| SAVI | −0.86 | 7.72 | −15.52 | 7.11 | 0.00 | −6.10 | 15.85 | −14.43 | 14.58 | 0.03 | −8.80 | 12.65 | −10.18 | 11.64 | 0.09 | 5.48 | 8.82 | −12.66 | 8.11 | 0.07 | −6.01 | 12.54 | −4.26 | 11.54 | 0.04 | −10.89 | 10.41 | −2.12 | 9.58 | 0.18 |
| EVI | 0.26 | 0.87 | −15.52 | 2.71 | 0.02 | −0.56 | 1.81 | −21.74 | 5.62 | 0.02 | 0.27 | 1.50 | −17.43 | 4.66 | 0.01 | −0.69 | 0.99 | −9.74 | 3.08 | 0.09 | 0.15 | 1.45 | −9.33 | 4.52 | 0.00 | 0.55 | 1.28 | −10.42 | 3.98 | 0.04 |
| SLAVI | −0.24 | 1.67 | −15.78 | 3.69 | 0.00 | −0.34 | 3.47 | −19.28 | 7.68 | 0.00 | −2.07 | 2.71 | −13.72 | 6.00 | 0.10 | 1.34 | 1.88 | −10.57 | 4.17 | 0.09 | −0.27 | 2.77 | −9.20 | 6.13 | 0.00 | −3.27 | 2.01 | −4.96 | 4.45 | 0.35 |
| NDRE | 4.36 | 11.66 | −18.60 | 6.16 | 0.03 | −1.76 | 24.58 | −19.10 | 12.98 | 0.00 | −8.51 | 19.90 | −13.77 | 10.51 | 0.04 | 5.49 | 13.77 | −10.52 | 7.28 | 0.03 | −7.38 | 19.34 | −5.90 | 10.21 | 0.03 | −21.29 | 14.78 | −0.90 | 7.81 | 0.29 |
| REIP | 0.06 | 0.19 | −60.20 | 137.78 | 0.02 | −0.08 | 0.40 | 39.75 | 288.15 | 0.01 | 0.08 | 0.33 | −76.51 | 236.98 | 0.01 | −0.09 | 0.22 | 57.00 | 162.10 | 0.03 | −0.12 | 0.31 | 79.18 | 227.38 | 0.03 | −0.28 | 0.25 | 192.19 | 185.60 | 0.20 |
| RNDVI | 8.05 | 16.54 | −19.61 | 6.80 | 0.05 | 6.83 | 35.06 | −22.83 | 14.41 | 0.01 | −19.39 | 27.67 | −10.30 | 11.37 | 0.09 | 15.26 | 18.83 | −13.89 | 7.74 | 0.12 | −6.51 | 27.92 | −7.11 | 11.48 | 0.01 | −30.88 | 21.03 | 0.55 | 8.65 | 0.30 |
| NDII | −6.17 | 10.57 | −14.18 | 3.68 | 0.06 | −1.36 | 22.70 | −19.56 | 7.90 | 0.00 | −11.65 | 17.97 | −14.23 | 6.26 | 0.08 | 5.70 | 12.67 | −9.60 | 4.41 | 0.04 | 2.44 | 18.08 | −10.62 | 6.30 | 0.00 | −24.68 | 11.90 | −3.60 | 4.14 | 0.46 |
| NDSI | 1.59 | 15.89 | −16.90 | 5.96 | 0.00 | 9.51 | 32.81 | −23.58 | 12.31 | 0.02 | −30.67 | 23.55 | −6.78 | 8.84 | 0.25 | 22.77 | 15.83 | −16.14 | 5.94 | 0.29 | 4.65 | 26.31 | −11.52 | 9.87 | 0.01 | −33.33 | 18.36 | 0.35 | 6.89 | 0.40 |
| SIWSI | 3.09 | 28.70 | −18.07 | 15.52 | 0.00 | −63.76 | 33.33 | 15.59 | 18.03 | 0.55 | 67.20 | 53.48 | −54.49 | 28.92 | 0.34 | −39.52 | 32.52 | 14.04 | 17.59 | 0.33 | −84.60 | 22.30 | 36.58 | 12.06 | 0.83 | 58.43 | 46.73 | −43.74 | 25.27 | 0.34 |
| ARVI | −0.30 | 9.24 | −16.05 | 8.04 | 0.00 | −14.11 | 18.15 | −7.78 | 15.79 | 0.11 | −12.00 | 14.89 | −7.83 | 12.96 | 0.11 | 4.34 | 10.76 | −11.40 | 9.36 | 0.03 | −9.91 | 14.67 | −1.18 | 12.77 | 0.08 | −14.19 | 12.18 | 0.21 | 10.60 | 0.21 |
| ARVI2 | 3.09 | 28.70 | −18.07 | 15.52 | 0.00 | −63.76 | 33.33 | 15.59 | 18.03 | 0.55 | 67.20 | 53.48 | −54.49 | 28.92 | 0.34 | −39.52 | 32.52 | 14.04 | 17.59 | 0.33 | −84.60 | 22.30 | 36.58 | 12.06 | 0.83 | 58.43 | 46.73 | −43.74 | 25.27 | 0.34 |
| GARI | 1.22 | 4.93 | −18.41 | 8.49 | 0.01 | −3.19 | 10.21 | −14.54 | 17.60 | 0.02 | 2.59 | 8.41 | −22.70 | 14.50 | 0.02 | −4.47 | 5.51 | 0.06 | 9.50 | 0.12 | 0.52 | 8.22 | −10.67 | 14.17 | 0.00 | 4.04 | 7.15 | −19.06 | 12.32 | 0.06 |

### Crop classification by optical data

Crop classification map derived from Sentinel-2 depicts most of the area under rice crop followed by orchard area. A few fallow regions were found, which are defined as agricultural landscapes. Still, the farmer did not grow the crop in the particular season due to the possibility as those are under highlands where water cannot stay and is not suitable for rice cultivation. Water bodies are dominant in the Southeast Jashore district; as this district is the border area of Bangladesh, very few settlement areas were found. Thus, accordingly, the Jashore district of Bangladesh is mainly an agricultural potential production area where rice is the dominant crop in Kharif/monsoon season.

The maximum likelihood classifier-based map is shown in Fig. 16, and this depicts the broad land-use land-cover map. Here, overall accuracy was 80%, and the kappa coefficient was 72.25. The results showed the potential of supervised classification similar to Singh et al. (2020), where they classified sugarcane crops using Indian Remote Sensing (IRS) satellite observed LISS-III sensor datasets.

### Evaluate the relationship between backscatter values with various optical-based indices

The results of the best-fitted linear regression equation parameters of all thirteen spectral indices versus VV and VH polarization backscatter values are illustrated in Table 4, Table 5, and Table 6 for early, late, and very late-transplanted rice, respectively. In the case of early transplanted rice type, September 15th data VV polarization dB value has the highest correlation with ARVI2 index with 0.81 $R^2$ value. In the case of late-transplanted rice, it was found that the highest $R^2$ value was 0.27, and this value for the regression model of July 17th VV polarization dB value with NDSI spectral index. In very late transplanted rice, the highest $R^2$ value was 0.83, and this value was found for the best regression model of the August 10th VV polarization dB value with ARVI2 and SIWSI indices. But most of the optical indices have shown moderate R2 with VH backscatter for the early sown rice; this coincides with the peak vegetative stage (1st fortnight of September). It may thus be inferred that the crop health parameters derived in the Sentinel-2 derived indices NDVI, ARVI, ARVI-2 at their post-1-month peak growth stages (October data) partially explain the backscatter response from the September 15th data. The correlation would have been stronger with the early September or August optical datasets, probably before the attainment of the peak stage, but unfortunately, cloud-free data were not available.

Also, the very late sown crop (end August planted), which are very few number fields, showed moderate response with SIWSI with September 15th VH polarization again due to the reasons mentioned above. They are in peak vegetative during mid-October or just before the peak stage in September. In addition, there is the coherence of response in VV-backscatter with the cross-poll response (Table 6) as the late crop manifested increasing response, unlike the early harvest where saturation occurred in VV-September 15th (Table 4). For this category of rice, SIWSI and ARVI2 are showing higher reactions with the August 10 data; this can be attributed either to the previous season's rice or vegetables grown before the current rice season.

Thus, we can say early transplanted rice VV polarization dB value correlates with the ARVI2 index, and late-transplanted rice VV polarization dB value significantly correlates with ARVI2 and SIWSI. Based on the regression outputs from different rice crop types with VV and VH polarization, it was observed that very late rice type backscatter values have the highest correlation with optical spectral vegetation indices, specially NDII, SIWSI, and ARVI2. These values may be used as a proxy of SAR data or vice-versa.

## Conclusions and recommendations

We attempted to categorize various rice types in temporal signatures of non-rice features, and backscatter values did not change over time. However, in the case of rice crop backscatter values, it increases over time. The first rice categories have been done using VV polarization. On adding VH polarization, more rice area has come as volume scattering component more captured by the cross-polarization response. The later stage saturation effect could be taken care of by the cross-polarization. The first classification approach used only VV polarization, the overall accuracy was 70%, but after adding VH polarization for rice, the overall accuracy increased up to 80%. Early transplanted rice covers a minimal area, about 4% of the total rice area. On the other hand, the late transplanted rice covers a vast area, about 62% of the total rice area (majority) picked up by the August SAR data. Very late transplanted rice covers about 33% of the total rice area. Most of the farmers transplanted their rice between late July and early August, some transplanted in mid-late August. Very few farmers could do the transplantation from mid to late July due to the late onset of rains. Total Aman rice area covered around 121,496 ha. According to the newest publication from the Bangladesh Bureau of Statistics (BBS 2017), in 2016–2017, total Aman rice area of Jashore district was 123,116 ha. Early and late transplanted rice VV polarization has good relation with ARVI2 indices.

Though the early transplanted rice was very sparsely found, its response and signature were prominently picked up by the cross-pol backscatter when the co-pol response was saturated. Their relationship, especially the VH backscatter with few indices, viz., the red edge indices, ARVI, and many others (Table 6), was moderate depicting. However, the peak response of the rice crop has faded away, but the structural/geometric manifestation left an imprint in VH polarization, being dynamic. For the late and very late sown crop, the manifestation was in VV-polarization though weaker in the former and moderate in the very late harvest due to perfect time synchronization with the optical data and captured the tillering stage/active-vegetative stage.

The transplantation map helps crop patterns and agro-climatic condition analysis of the area. Also, the findings from the synergistic use of SAR and optical data are novel and give us insight into a holistic understanding of the crop's micro and macro-structure. This will add to the appropriate field and human resources allocation for crop management, mainly when unavailable temporal data. There is further need to extend by adding temporal optical data at suitable phenological stages for inventory and other crops over years and seasons. It will give a complete cropping pattern scenario of that area.

## Declarations

**Conflict of interest** The authors declare no competing interests.

## References


Adamu B, Tansey K, Ogutu B (2018) Remote sensing for detection and monitoring of vegetation affected by oil spills. Int J Remote Sens 39(11):3628–3645

Alebele Y, Zhang X, Wang W, Yang G, Yao X, Zheng H, Zhu Y, Cao W, Cheng T (2020) Estimation of canopy biomass components in paddy rice from combined optical and SAR data using multi-target Gaussian regressor stacking. Remote Sens 12(16):2564

Awal MA, Siddique MAB (2011) Rice production in Bangladesh employs by ARIMA model. Bangladesh J Agric Res 36(1):51–62

Banglapedia. Dhaka. Asiatic Society of Bangladesh (2020) https://en.banglapedia.org/index.php/Jessore_District. Accessed 3 Mar 2019

Barnes EM, Clarke TR, Richards SE, Colaizzi PD, Haberland J, Kostrzewski M, Waler P, Choi C, Riley E, Thompson LT (2000) Coincident detection of crop water stress, nitrogen status and canopy density using ground based multispectral data, vol 1619. In Proceedings of the Fifth International Conference on Precision Agriculture, Bloomington, MN, USA

[BARC] Bangladesh Agricultural Research Council, http://cropcalendar.barcapps.gov.bd/index.php

[BBS] Bangladesh Bureau of Statistics (2017) Planning Division, Government of the People's Republic of Bangladesh, Year Book of Agricultural Statistics. Dhaka

[BRRI] Bangladesh Rice Research Institute (2018) Ministry of Agriculture, Government of the People's Republic of Bangladesh, Audhunikdhaner chas [Mordern rice cultivation]

Choudhury I, Chakraborty M, Santra SC, Parihar JS (2012) Methodology to classify rice cultural types based on water regimes using multi-temporal RADARSAT-1 data. Int J Remote Sens 33(13):4135–4160

Chakraborty M, Panigrahy S, Sharma SA (1997) Discrimination of rice crop grown under different cultural practices using temporal ERS-1 synthetic aperture radar data. ISPRS J Photogramm Remote Sens 52(4):183–191. https://doi.org/10.1016/S0924-2716(97)00009-9

Dave R, Haldar D, Dave V, Manjunath KR, Pandey V (2017) Crop monitoring and classification using multitemporal polarimetric SAR (RISAT-1) data for cotton and groundnut crops of Gujarat. J Agrometeorol 19(Special Issue):171–178

[ESA] European Space Agency (2013) Sentinel-1 user handbook. [ESA Standard Document]. European Commission, European Union. https://sedas.satapps.org/wp-content/uploads/2015/07/Sentinel-1_User_Handbook.pdf

[ESA] European Space Agency (2021) Sentinel-2 products specification document, Copernicus-Sentinel-2, Issue-14.6

[ESA] European Space Agency (2022) Copernicus, user guide. https://sentinels.copernicus.eu/web/sentinel/user-guides/sentinel-2-msi/processing-levels/level-2

Faisal BM, Rahman H, Sharifee NH, Sultana N, Islam MI, Ahammad T (2019) Remotely sensed boro rice production forecasting using MODIS-NDVI: a Bangladesh perspective. AgriEngineering 1(3):356–375

Friedl MA, Brodley CE (1997) Decision tree classification of land cover from remotely sensed data. Remote Sens Environ 61(3):399–409

Fontanelli G, Paloscia S, Zribi M, Chahbi A (2013) Sensitivity analysis of X-band SAR to wheat and barley leaf area index in the Merguellil basin. Remote Sens lett 4(11):1107–1116. https://doi.org/10.1080/2150704X.2013.842285

Ghaffarian S, Kerle N, Filatova T (2018) Remote sensing-based proxies for urban disaster risk management and resilience: a review. Remote Sens 10(11):1760

Gumma MK, Thenkabail PS, Maunahan A, Islam S, Nelson A (2014) Mapping seasonal rice cropland extent and area in the high cropping intensity environment of Bangladesh using MODIS 500 m data for the year 2010. ISPRS J Photogramm Remote Sens 91:98–113

Haldar D, Patnaik C (2010) Synergistic use of multi-temporal Radarsat SAR and AWiFS data for Rabi rice identification. J Indian Soc Remote Sens 38(1):153–160

Haldar D, Das A, Mohan S, Pal O, Hooda RS, Chakraborty M (2012) Assessment of L-band SAR data at different polarization combinations for crop and other landuse classification. Progress Electromagn Res 36:303–321

Haldar D, Patnaik C, Mohan S, Chakraborty M (2012) Jute and tea discrimination through fusion of SAR and optical data. Progress Electromagn Res B 39:337–354

Haldar D, Patnaik C, Chakraborty M (2014) Jute crop discrimination and biophysical parameter monitoring using multi-parametric SAR data in West Bengal. India Oalib 01(06):1–11. https://doi.org/10.4236/oalib.1100817

Haldar D, Manjunath KR, Panigrahy S, Jain V, Gopalan RS, Khullar M, Chakraborty M, Parihar JS (2014) Monsoon paddy monitoring and assessment using synthetic aperture radar data under BGREI programme in Odisha, India. Paddy Water Environ 13(4):343–352

Haldar D, Chakraborty M (2019) Characterization of monsoon and summer season paddy transplantation date in India using RISAT-1 synthetic aperture radar. Geocarto Int 36(10):1178–1192

Haldar D, Tripathy R, Dave V, Dave R, Bhattacharya BK, Misra A (2020) Monitoring cotton crop condition through synergy of optical and radar remote sensing. Geocarto Int 37(2):377–395

Herrmann I, Pimstein A, Karnieli A, Cohen Y, Alchanatis V and Bonfil JD. (2010) Utilizing the vensus red-edge bands for assessing LAI in crop fields. Core Spatial Databases-Updating, Maintenance and Services-from Theory to Practice

[IDB] Index database. 2020a. https://www.indexdatabase.de/db/i-single.php?id=89

[IDB] Index database. 2020b. https://www.indexdatabase.de/db/i-single.php?id=4

Kabir MS, Salam MU, Islam AKMS, Sarkar MAR, Mamun MAA, Rahman MC, Nessa B, Kabir MJ, Shozib HB, Hossain MS, Bhuiyan MKA, Karmakar B, Rahman MS, Haque MM, Khatun MT, Ali MP, Rabbi SMHA, Biswas PL, Rashid ESMH, Rahman NMF (2020) Doubling rice productivity in Bangladesh: A way to achieving SDG 2 and moving forward. Bangladesh Rice Journal 24(2):1–47

Liang S, Schaepman M, Kneubühler M (2008) Remote sensing signatures: Measurements, modeling and applications. In: Advances in photogrammetry, remote sensing and spatial information sciences: 2008 ISPRS congress book, vol 7. CRC Press, p 127. https://doi.org/10.1201/9780203888445

Li P, Jiang L, Feng Z, Sheldon S, Xiao X (2016) Mapping rice-cropping systems using Landsat-derived renormalized index of normalized difference vegetation index (RNDVI) in the Poyang Lake Region. China Front Earth Sci 10(2):303–314

Mamun MAA, Nihad SAI, Sarkar MAR, Aziz MA, Qayum MA, Ahmed R, Rahman NMF, Hossain MI, Kabir MS (2021) Growth and trend analysis of area, production and yield of rice: A scenario of rice security in Bangladesh. PLOS ONE 16(12):1–18

Macelloni G, Paloscia S, Pampaloni P, Gai M (2001) The relationship between the backscattering coefficient and the biomass of narrow and broad leaf crops. IEEE Trans Geosci Remote Sens 39(4):873–884. https://doi.org/10.1109/36.917914

McNairn H, Kross A, Lapen D, Caves R, Shang J (2014) Early season monitoring of corn and soybeans with TerraSAR-X and RADARSAT-2. Int J Appl Earth Obs Geoinf 28:252–259

McNairn H, Deguise JC, Secker J, Shang J (2001a) Development of remote sensing image products for use in precision farming. In: Submitted to Third European Conference on Precision Farming, Montpellier, France, pp 18–20

McNairn H, Duguay C, Boisvert J, Huffman E, Brisco B (2001b) Defining the sensitivity of multi-frequency and multi-polarized radar backscatter to post-harvest crop residue. Can J Remote Sens 27(3):247–263

Nguyen DB, Wagner W (2017) European rice cropland mapping with Sentinel-1 data: the Mediterranean region case study. Water 9(6):392

Nuevo RU, Saludes RB, Dorado MA, Bantayan NC (2017) Monitoring of rice in small paddy fields using multi-temporal sentinel-1 data. 38th Asian Conference on Remote Sensing - Space Applications: Touching Human Lives, ACRS 2017, pp 1–10

Olsen JL, Ceccato P, Proud SR, Fensholt R, Grippa M, Mougin E, Ardo J, Sandholt I (2013) Relation between seasonally detrended shortwave infrared reflectance data and land surface moisture in semi arid sahel. Remote Sens 5(6):2898–2927

Park H, Choi J, Park N, Choi S (2017) Sharpening the VNIR and SWIR bands of Sentinel-2A imagery through modified selected and synthesized band schemes. Remote Sens 9(10):1080

Rahman MC, Pede V, Balie J, Pabuayon IM, Yorobe JM, Mohanty S (2020) Assessing the market power of millers and wholesalers in the Bangladesh rice sector. J Agribusiness Dev Emerg Econ 11(3):280–295. https://doi.org/10.1108/JADEE-04-2018-0053

Rahman MC, Pede VO, Balié J (2022) Welfare impact of asymmetric price transmission on rice consumers in Bangladesh. Rev Dev Econ 26(3):1600–1617

Sahu H, Haldar D, Danodia A, Kumar S (2018) Classification of orchard crop using sentinel-1A synthetic aperture radar data. Int Arch Photogramm Remote Sens Spat Inf Sci 42:335–338

Shanmugapriya S, Haldar D, Danodia A (2020) Optimal datasets suitability for pearl millet (Bajra) discrimination using multiparametric SAR data. Geochem Int 35(16):1814–1831

Shewalkar P, Khobragade A, Jajulwar K (2014) Review paper on crop area estimation using SAR remote sensing data. IOSR J Electr Electron Eng 9:97–98

Sibandze P, Mhangara P, Odindi J, Kganyago M (2014) A comparison of normalised difference snow index (NDSI) and normalised difference principal component snow index (NDPCSI) techniques in distinguishing snow from related land cover types. South Afr J Geomatics 3(2):197–209

Susantoro TM, Wikantika K, Saepuloh A and Harsolumakso AH. (2018) Selection of vegetation indices for mapping the sugarcane condition around the oil and gas field of North West Java Basin, Indonesia. In IOP Conference Series Earth and Environmental Science (Vol. 149, No. 1, p. 012001). IOP Publishing

Singh R, Patel NR and Danodia A (2020) Mapping of sugarcane crop types from multi-date IRS-Resourcesat satellite data by various classification methods and field-level GPS survey. Remote Sens Appl: Soc Environ. https://doi.org/10.1016/j.rsase.2020.100340

Sriwongsitanon N, Gao H, Savenije HHG, Maekan E, Saengsawan S, Thianpopirug S (2015) The Normalized Difference Infrared Index (NDII) as a proxy for soil moisture storage in hydrological modelling. Hydrol Earth Syst Sci Discuss 12(8). https://doi.org/10.5194/hessd-12-8419-2015

Thenkabail PS, Smith RB, De Pauw E (1999) Hyperspectral vegetation indices for determining agricultural crop characteristics, CEO research publication series No. 1. Center for Earth Observation, Yale University Press, New Haven

Xue J, Su B (2017) Significant remote sensing vegetation indices: a review of developments and applications. J Sens 2017:1–17

Zuzulova V, Vido J (2018) Normalized difference vegetation index as a tool for the evaluation of agricultural drought in Slovakia. Ecocycles 4(1):83–87